ISTFA 2023: Proceedings of the 49th International
Symposium for Testing and Failure Analysis Conference
November 12—16, 2023, Phoenix, Arizona, USA
https://doi.org/10.31339/asm.cp.istfa2023p0483

Check for updates

Copyright © 2023 ASM International®
All rights reserved.
www.asminternational.org

SiC MOSFET micro-explosion due to a Single Event Burnout: analysis at the device and die levels

COQ GERMANICUS Rosine
NORMANDIE UNIV, ENSICAEN, UNICAEN, CNRS, CRISMAT, 14000 Caen, France
rosine.germanicus@unicaen.fr

PHULPIN Tanguy
Université Paris-Saclay, CentraleSupélec, CNRS, GeePs, Sorbonne Université, 91192, Gif-sur-Yvette, 75252, Paris, France
tanguy.phulpin@centralesupelec.fr

ROGAUME Thomas
Institut Pprime, UPR 3346 CNRS, Université de Poitiers, ISAE-ENSMA, Chasseneuil du Poitou, France
thomas.rogaume@univ-poitiers.fr

NISKANEN Kimmo
Accelerator Laboratory, Department of Physics, University of Jyvaskyla, FIN-40014 Jyvaskyla, Finland
kimmo.h.niskanen@jyu.fi

FROISSART Sandrine
NORMANDIE UNIV, ENSICAEN, UNICAEN, CNRS, CRISMAT, 14000 Caen, France
sandrine.froissart@ensicaen.fr

LATRY Olivier
Groupe de Physique des Matériaux, Normandie Université, UNIROUEN, INSA Rouen, CNRS UMR 6634, 76000 Rouen, France
olivier.latry@univ-rouen.fr

MICHEZ Alain
Institut d'Electronique et des Systèmes (IES), Université de Montpellier, UMR-CNRS 5214, Montpellier, 34095 France
alain.michez@umontpellier.fr

LÜDERS Ulrike
NORMANDIE UNIV, ENSICAEN, UNICAEN, CNRS, CRISMAT, 14000 Caen, France
ulrike.luders@ensicaen.fr

Abstract

For device qualification in harsh environments (space, avionic and nuclear), radiation testing identifies the sensitivity of the devices and technologies and allows to predict their degradation in these environments. In this paper, the analysis of the electrical characteristics and of the failure of a commercial SiC MOSFET after a Single Event Burnout (SEB) induced by proton irradiation are presented. The goal is to highlight the SEB degradation mechanism at the device and die levels. For failed devices, the current as a function of the drain-source bias (V_{DS}) in off-state (V_{GS}=0V) confirms the gate rupture. For the die analysis, Scanning Electron Microscopy (SEM) investigations with energy-dispersive X-ray spectroscopy (EDX) analysis reveals the trace of the micro-explosion related to the catastrophic SEB inside the SiC die. With a fire examination, similar to a blast, the SEM analysis discloses damages due to the large local increase of the temperature during the SEB thermal runaway, leading to the thermal decomposition of a part of the SiC MOSFET and the combustion with gaseous emissions in the device structure.

Introduction

Nowadays, Silicon carbide (SiC) is a mature wide band-gap semiconductor employed for high-efficiency power technologies, such as in electrical vehicles [1]. The wide band

Downloaded from http://dl.asminternational.org/istfa/proceedings-pdf/ISTFA2023/84741/483/662579/istfa2023p0483.pdf
by guest

gap of this material allows for a reduction of device sizes, weights and switching losses [2]. Besides, the high thermal conductivity of SiC facilitates its use in harsh environments such as power switch for nuclear applications (space, avionic, nuclear reactor and military). Nevertheless, while the fourth generation of SiC MOSFETs has just been designed, its adoption for space applications stays rare [3], [4]. Despite the robustness of the SiC material, the catastrophic effects due to space environment radiation were demonstrated and analyzed [2-3]. SiC devices are sensitive to Single Event Burnouts (SEB) [7]–[10], Single Event Gate Ruptures (SEGR) [11], [12] and single event leakage current (SELC)[13]. In SiC MOSFETs, due to the extreme internal drain to source electric field through the SiC, unsuited currents can induce a thermal runaway. This phenomenon can lead to the breakdown of power devices and to a loss of device functionality. For destructive SEB, a primary particle (as a neutron, proton or ion) impacts on the device, therefore ionizing secondary particles can be created inside. Along the trajectory of this secondary particle, electron and hole pairs are generated. Since the electric field to the SiC is 10 times higher than in Si MOSFETs, the power heat density in the SiC is 100 times higher and triggers the impact ionization. The strongly localized and therefore high-density current can generate a thermal transient and runaway which leads to the catastrophic failure. Impacts of several parameters such as the nature of the particle [14], [15], energy, linear energy transfer (LET)[8], device technology [7], bias voltage (V_{DS} and V_{GS}) [16], [17] during irradiation and post-electrical stress have been investigated. Previous studies show that the SEB sensitivity increases with the applied the drain-source bias (V_{DS}) during the irradiation due to the increasing electric field in the drift layer of the MOSFET [16], [17]. In [18], authors propose a mapmaking of the type of damages (oxide latent damage, degradation, crystal latent damage and SEB) as a function of the V_{DS} and the LET. On top of the catastrophic failure, for the devices irradiated with protons which did not exhibit SEB, an irradiation-induced gate oxide degradation has been observed in the post-irradiation stress tests [19]. And for heavy-ions, the decomposition of the SiC crystal lattice was revealed after a post-irradiation V_{DS} sweep, in the pre-SEB region for SiC MOSFET bare dies [18].

In this paper, a failure analysis of a COTS packaged SiC MOSFET after SEB induced by proton radiation is presented, at the device and die levels. A failure analysis flow chart is established, the results, analysis and risk assessment (for successful analysis) at each step are presented. After the analysis of the electrical I-V characteristics, Scanning Electron Microscopy (SEM) investigations with energy-dispersive X-ray spectroscopy (EDX) reveal the local micro-explosion phenomenon in the SiC die. Based on the analysis of the traces of the thermal blast, explanations of the micro-explosion are formulated.

Technical Description

Devices

The devices under test (DUTs) are packaged, commercial SiC power VD-MOSFETs. Dedicated for renewable energy applications and high voltage DC/DC converters, the device is a classical 4H-SiC planar n-channel 1.2 kV MOSFET with on-resistance of 350 mΩ in a TO-247 package with 3 pins. The permanent nominal current between drain-source is 7.6 A and 20 A for a pulsed drain current. Electrical measurements, including forward and reverse characterizations, have been performed before and after irradiation for each device electrical characterizations using the Keysight 2461 SMU at room temperature.

Device Irradiation

To evaluate devices sensitivity against proton particles at medium energies, proton irradiations were performed at the RADiation Effects Facility (RADEF) in the Accelerator Laboratory at the University of Jyväskylä, Finland. For this accelerated SEB test, during irradiations, a drain-to-source voltages (V_{DS}) of about 1000 V (83 % of the maximum rating) was applied and the gate and source were grounded (V_{GS} =0V) using a Keysight 2470 SMU. These bias settings have been chosen to ensure the creation of SEB phenomena [16]. The test circuit is similar to the experiment described in [19], where DUTs were connected in parallel to the high voltage. The 53 MeV proton beam was obtained from the K130 cyclotron. For this experiment, the proton beam flux was 10^8 cm^{-2} s^{-1} with 10% uncertainty on the DUT area. The total protons fluence reached 10^{11} p/cm^{-2}.

Results

Failure flow chart and risk assessment

For a thorough understanding of the SEB mechanism induced by the primary proton at the SiC device and die levels, the proposed experimental flow chart (Fig.1) presents two main parts: first, an experimental statistic procedure is used to create the SEB for the irradiated devices and the electrical characteristics of the irradiated device are monitored. Second, the failure analysis itself is carried out to reveal the type of defect at the die level. In addition, at each step of the flow chart, the risk assessment level for the success is evaluated. For the analysis at the die level, the challenge is to open the packaging to identify the failure location. For this, the failure flow chart presents several steps: 1) opening of the package for the SiC die location in an unknown device geometry, 2) identification and isolation of the damage area induced by the protons, 3) preparation of a cross section surface for the SEM microscope, 4) the characterization. The sample preparation steps (1-3) are those with the highest risk. In fact, during sample preparations, mechanical stresses and strains are necessary to obtain the access to the damaged areas. SiC is of high mechanical strength (800 MPa), very hard (hardness of 2800 Kg/mm² and a fracture toughness KIC of 4.6 $MPa.m^{1/2}$), but also a very fragile material. Therefore, it was necessary to identify adapted

Downloaded from http://dl.asminternational.org/istfa/proceedings-pdf/ISTFA2023/84741/483/662579/istfa2023p0483.pdf
by guest

techniques and sample treatments, in order to single out the damaged area without inducing supplementary mechanical damage during the sample preparation. At the different stages risks are assessed: a wrong chip location, debonding of the SiC die, additional defects created by the mechanical preparation, milling tool breakage, difficulty in precisely locating the damage zone or the SiC die break.

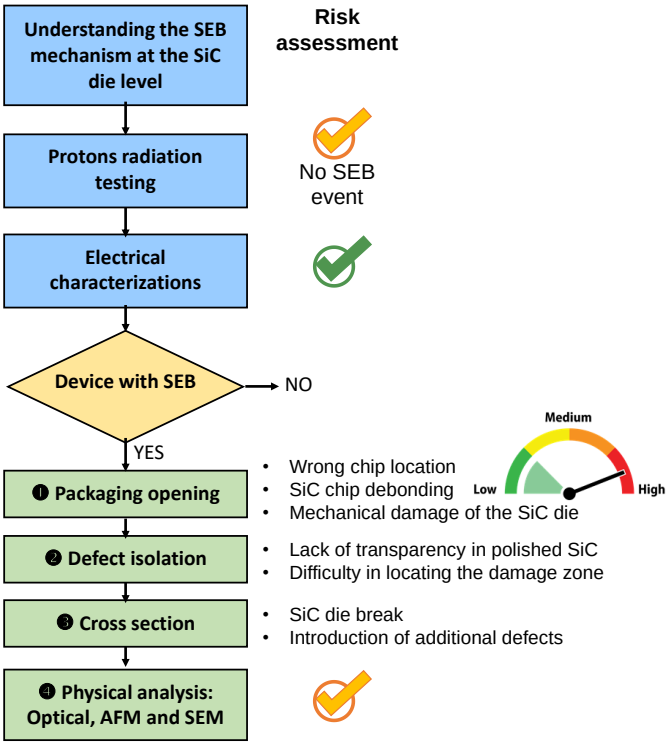

Figure 1: Failure analysis flow chart to determine the mechanism of the SEB in a packaged SiC MOSFET. Steps of the flow chart and risk assessment are indicated

SEB event detection during radiation

During proton irradiation of the DUTs, the online drain current (I_D) of the ten devices was monitored in parallel. All details of the experimental procedure are given in [9].

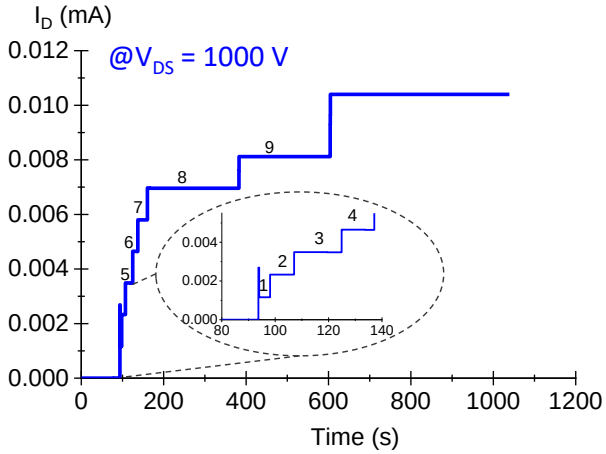

Figure 2: Evolution of the online current I_D during proton irradiation at 53 MeV of all ten SiC MOSFET DUTs in parallel.

A SEB event is detected by the sudden increase of the current. Notes that for isolation, a current-limiting resistance is used for each MOSFET. Fig. 2. shows the current change as a function of the irradiation time, related to the fluence of protons. The monitoring of the drain current I_D during the irradiation showed that nine devices have suffered from probable catastrophic SEB-type degradation. Four of these SiC MOSFETs were randomly selected for the further failure analysis. An analysis of the statistical properties of the SEB mechanism by applying Weibull statistics is presented in [19] indicating random failure over time, for this device irradiated with 53 MeV protons.

Electrical signatures of the SEB

The evolution of the I_D as a function of the V_{DS} in off-sate (V_{GS}=0 V) is plotted for four failed devices (Fig.3). The electrical characteristics of the device after SEB are compared to the pristine SiC MOSFET.

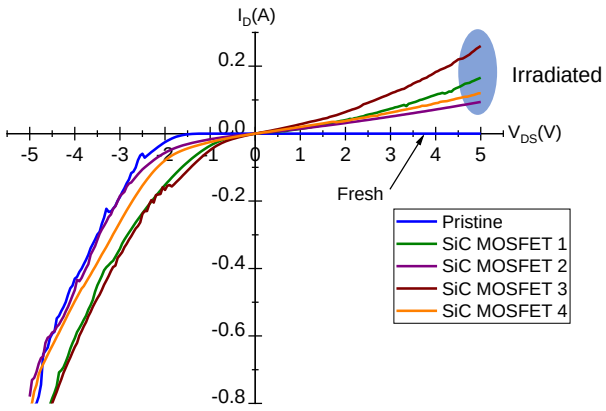

Figure 3: I_D-V_{DS} characteristics of the irradiated and failed devices. Characteristic are compared with a fresh device.

Downloaded from http://dl.asminternational.org/istfa/proceedings-pdf/ISTFA2023/84741/483/662579/istfa2023p0483.pdf
by guest

As expected, a conductive trend (I_D-V_{DS}) is measured after SEB. The electrical signature of the catastrophic SEB is then, the presence of a non-negligible current in direct polarization, even under small polarization from 500 mV. A variability between the four devices is measured. By comparing with the pristine device, the MOSFET channel control of the failed devices is lost. This result indicates catastrophic damage at the device gate. At V_{DS} = 4 V (Fig. 3), the current exceeds 0.1 A for all damaged DUTs after the irradiation. This strongly suggests that at the SiC die level, the degradation of the material produces a conductive pathway through the MOSFET structure and leads to a high leakage current in forward mode. Since the SiC MOSFET has internal diode formed by the P-I-N layers, this device presents the capacity to have reverse conduction. Interestingly, in reverse voltage I_D-V_{DS} characteristics, a survival of the diode characteristics of the SiC MOSFET is observed. The semi-log plot (Fig.4) shows that for V_{DS} = -0.6 V, the average measured leakage current is 14 mA for the degraded devices instead of 1.1 nA for the pristine one.

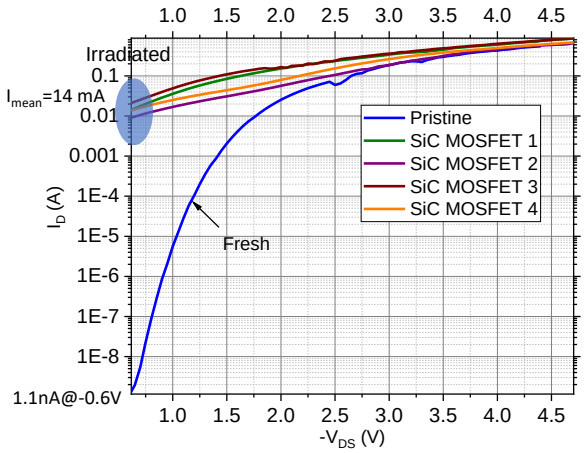

Figure 4: Reverse characterization at V_{GS}=0V of four failed MOSFETs compared to the pristine device, for reverse bias.

Furthermore, measurements of the drain, source and gate currents as a function of gate bias (V_{GS} with relative low values) for V_{DS}=0V, after irradiation (Fig.5), confirm the gate rupture: the gate current is high for forward and reverse V_{GS} bias. Comparing to the drain current, this characteristic shows that the I_D current flows mainly horizontally through the source and not through the epitaxial layer and the substrate (drain contact). After SEB a conductive patch is created locally between the gate and source contacts.

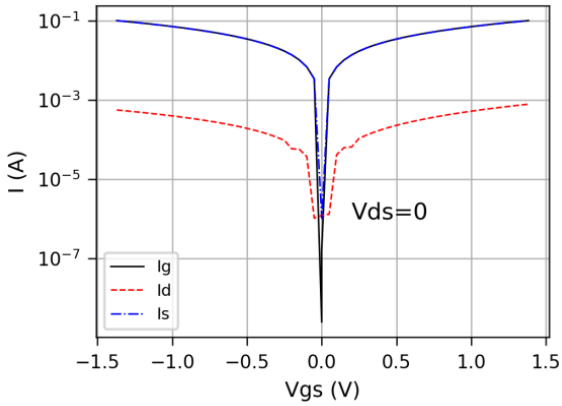

Figure 5: I_G, I_D and I_S as a function of gate bias for the irradiated device. A leakage has been triggered between Gate and Source.

With greater accuracy, considering the VD-MOSFET structure [20] of the device, after SEB, the failed devices present equivalent resistances between gate, source and drain contacts modified.
In addition, the same currents were measured as a function of drain bias after irradiation (Fig.6). The current flowing from drain to source shows that the p-type area below the gate has also been destroyed.

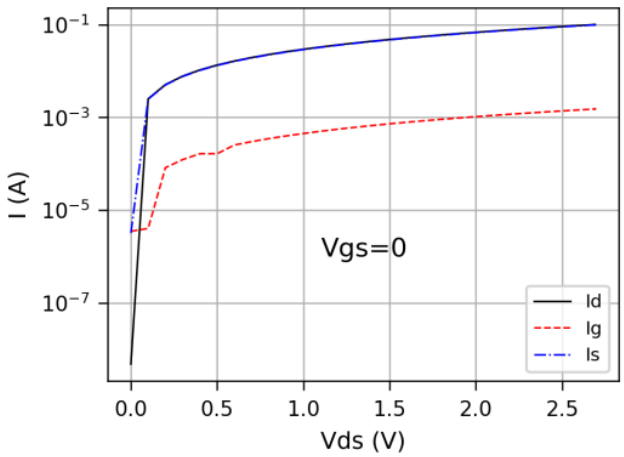

Figure 6: I_G, I_D and I_S as a function of drain bias for the irradiated device. A leakage has been triggered between drain and source.

Packaging opening

For the SiC die inspection, the device package is opened from the back side with a micro milling machine. The photo of the Fig. 7 illustrates the milling step, which consists to decapsulate de device.

Downloaded from http://dl.asminternational.org/istfa/proceedings-pdf/ISTFA2023/84741/483/662579/istfa2023p0483.pdf
by guest

Figure 7: Illustration of the milling step for a similar power SiC device (trial on similarly packaged device).

The structure of the studied package is shown in the optical view of a device in cross section. This optical view is obtained on a sacrificial device from the same batch. The nature of the materials can be distinguished (Fig.8): mold EMC (Epoxy Moulding Component) for packaging, SiC die with the die attaches and the copper base plate at the back side.

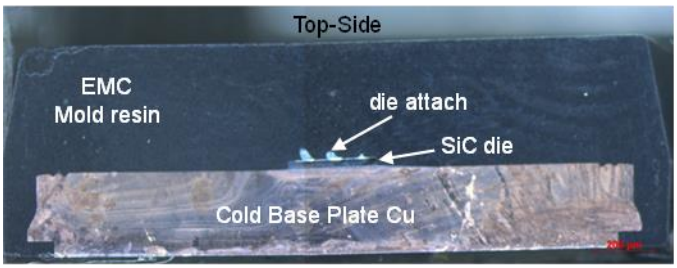

Figure 8: Cross sectional view of a sacrificial device

In order to expose the die as little as possible to mechanical strain, the Cu back plate was opened at the location of the SiC die. First, a laser was used for the removal of the Cu plate, and afterwards a mechanical tool. For the last step, a diamond tool was used for the thinning of the SiC die itself. Based on tests performed on the sacrificial component, the applied force and the milling velocity were adapted in order to avoid any inherent preparation defects.

Defect at the die level

From the back-side, the thinning of the SiC chip face allows to locate the area of the defect through the transparency of the thin SiC die. This step represents a high risk, since SiC material is a rigid but brittle material. Its mechanical behavior is close to that of glass. Three of the four devices were broken at this stage of the sample preparation. SiC thinning from a thickness of 170 µm to about 30 µm was necessary to allow a good optical inspection through the SiC die. Fig.9 represents the optical inspection of a failed die. The die is isolated from the copper base plate (1). The damage consists of a longitudinal crack in the middle surrounding an area with multiple radial cracks (2). The defect occupies a circular area with a diameter of more than 280 µm (3). Through the thinned SiC, a first black crown at the center and radial propagation traces can be observed (4).

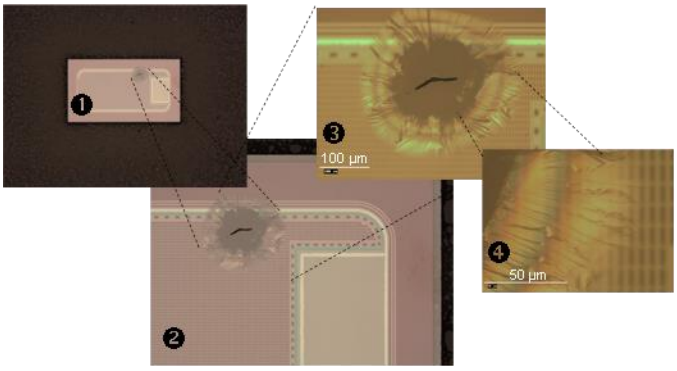

Figure 9: Optical inspection of the failed die after thinning

SEB defect at the SiC die level

A mechanical cross section was prepared at the end of the sample preparation. Backscattered electron (BSE) imaging and energy dispersive X-ray spectroscopy (EDX) mapping were performed using a scanning electron microscope (SEM, JSM-7200F JEOL). A large view (with a relative magnification of 330, for a size of 360 µm × 280 µm) of the cross-section surface is reported in Fig. 10. At the interface between the EMC and the SiC die a cavity (area dark on Fig.10) is identified. Just below, the row of SiC MOSFETs is completely destroyed. In addition, a round-shaped area (which seems to have been melted) is observed in the SiC material. The observation of the large crack (280 µm, indicated by the red arrows) inside the SiC semiconductor confirms that during the cross-sectional preparation, the cross-sectional stage has not caused any additional damage. This is the area shown on the backside on the Fig.9. A close up of the defect at the SiC die level is reported in Fig.11 a). At the top of the image, the mold EMC, the SiC MOSFET structure and the large crack in the SiC material can be observed. The outline image (Fig. 11b)), generated from the SEM view, allows to highlight the areas with strong deformation and therefore the collapse of the contact metal.

Under of the observed cavity, the different functional parts of the MOSFET structure are indicated in Fig. 11 b). The crack is located in the SiC substrate. The metallic source contact, just on top of the epilayer, is collapsed under the cavity, while at the left side, a swelling is observed.

Downloaded from http://dl.asminternational.org/istfa/proceedings-pdf/ISTFA2023/84741/483/662579/istfa2023p0483.pdf
by guest

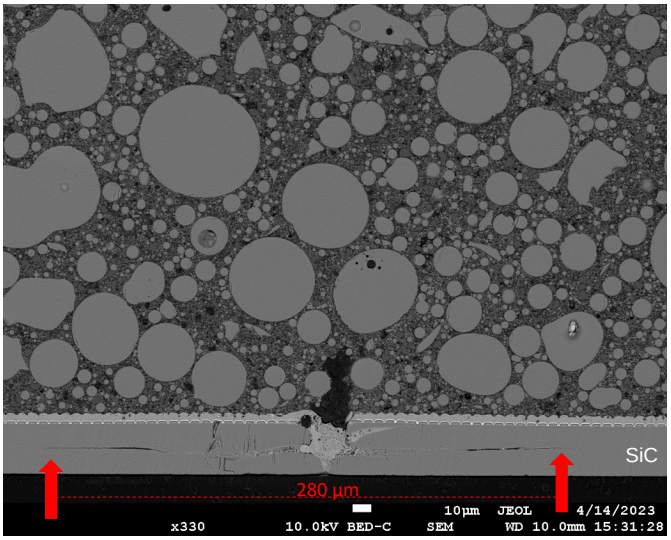

Figure 10: SEM view of the obtained cross section with backscattered electron detector.

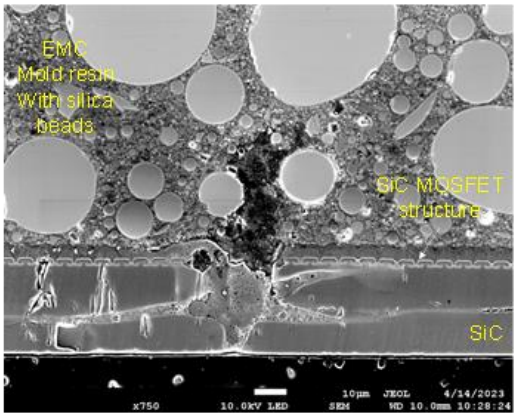

a)

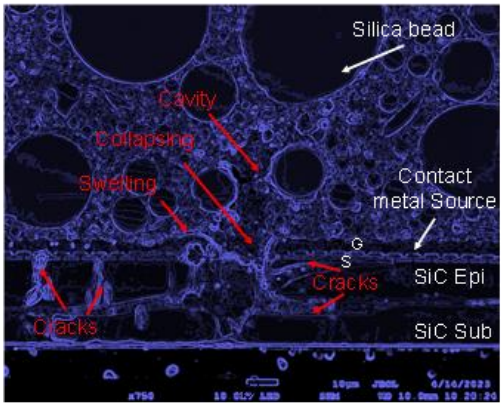

b)

Figure 11: (a) SEM view of the catastrophic degradation induced by the proton at the SiC die level, the SEM observation is zoomed on the damage in the gates region, at the center of the Fig.10 and (b) the generated contours image used for the analysis.

In order to identify the nature of the materials, EDX analysis was performed. The signals of the carbon, oxygen, aluminum and silicon are superimposed to the SE-SEM view (Fig. 12). For each element, the cartography is also represented.

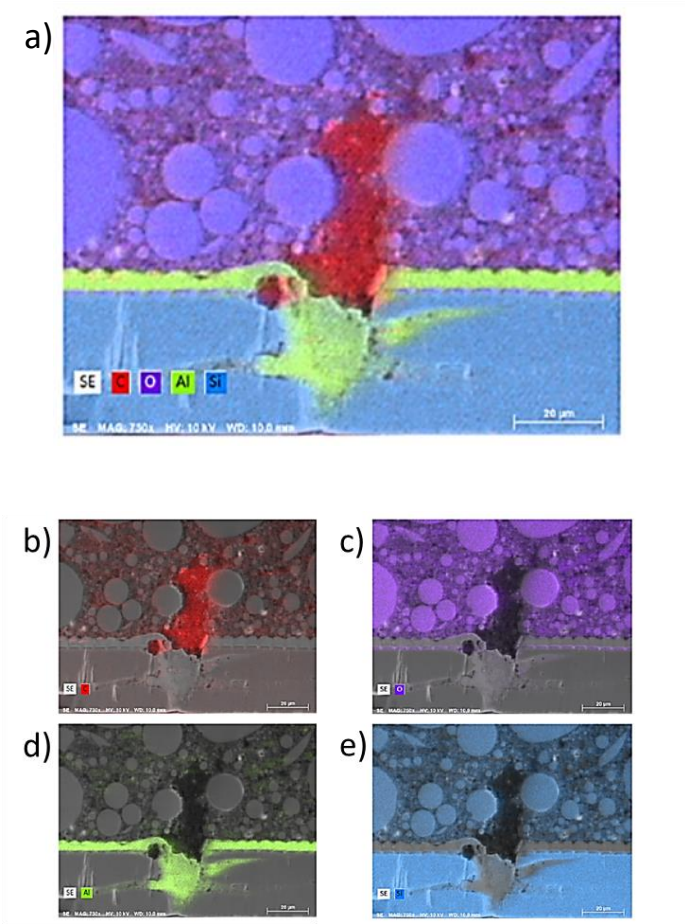

Figure 12: EDX measurements superimposed to the SEM view of the SiC cross section after the proton SEB. (a) the combined image for C (red), O (violet), Al (green), and Si. (blue) (b) EDX mapping of C. (c) EDX mapping of Si. (d) EDX mapping of O. (e) EDX mapping of Al.

A micro-explosion inside the SiC die

The location, isolation and analysis of the damage reveals the destruction of the SiC MOSFET and the defect inside the SiC semiconductor structure. EDX analysis reveals traces of carbon like a fire-place, indicating the occurrence of a micro-explosion. To better understand this micro-explosion, the local failure mechanism is correlated with the fire triangle. Indeed, in order to have combustion, it is necessary to have fuel, one oxidant (such as oxygen) and enough energy to initiate the reaction of combustion. In our present case, the proton SEB event generates in the SiC structure a high increase of local

Downloaded from http://dl.asminternational.org/istfa/proceedings-pdf/ISTFA2023/84741/483/662579/istfa2023p0483.pdf
by guest

temperature conducting to thermal decomposition of the SiC element. As oxygen is trapped in the MOSFET structure and EMC micro-pores, the energy transferred by the irradiation is sufficient, so combustion and thus explosion can take place. This is clearly visible in Fig. 12. High temperatures are reached, during the blast, when the local temperature exceeds the sublimation temperature of the SiC (> 2100 °C). The SiC epitaxial layer explodes, a cavity is created and is filled with the fusion of the aluminum layer (Fig. 12-f). The evidence of the combustion gas emissions is found in Fig.12-a) where a large concentration of Carbon is measured in the EMC packaging above the location of the SEB event. Failure analysis at the die level of a failed device after proton irradiation indicates micro-explosion like a thermal blast occurring during the SEB. The molten aluminum fills the cavity and creates new conductive path within the device, which is validated by the observed leakage current in the I-V characteristics.

Conclusions

The electrical characterization of a proton irradiated SiC MOSFET after SEB event has shown the creation of a conductive pathway inside the semiconductor, leading to the loss of off state of the device. Indeed, the pristine device shows a negligible off - current, while the four damaged DUTs show a substantial current in the off state. By the local damage analysis, the creation of cracks, cavity, micro-explosion marks and traces of CO_2 (attested by the EDX identification) have been examined. A local current path through the molten aluminum is measured at device off-state. EDX elemental mapping of the failed die location indicates a micro-explosion due to thermal effects, induced by the high bias voltage and the SiC properties. The observed area shows characteristic signatures of a combustion process. This analysis does not only explain the observed electrical failure of the SiC device, but indicates the inherent behavior of each material of the component during the SEB mechanism.

Acknowledgments

Authors would like to thank Clement Hodeau from Kummers and Xavier Larose from CRISMAT-UMR6508 Laboratory. The authors also would like to thank CARNOT ESP Institute for supporting the SiCAgeing research project.

References

[1] P. J. Wellmann, "Power electronic semiconductor materials for automotive and energy saving applications–SiC, GaN, Ga2O3, and diamond," *Zeitschrift für anorganische und allgemeine Chemie*, vol. 643, no. 21, pp. 1312–1322, 2017.

[2] A. Hussein, A. Castellazzi, P. Wheeler, and C. Klumpner, "Performance benchmark of Si IGBTs vs. SiC MOSFETs in small-scale wind energy conversion systems," in *2016 IEEE International Power Electronics and Motion Control Conference (PEMC)*, Sep. 2016, pp. 963–968. doi: 10.1109/EPEPEMC.2016.7752124.

[3] X. Jie, K. Qing, Z. Xuan, and L. Feng, "Application Prospect of SiC Power Semiconductor Devices in Spacecraft Power Systems," in *2017 13th IEEE International Conference on Electronic Measurement & Instruments (ICEMI)*, Oct. 2017, pp. 185–190. doi: 10.1109/ICEMI.2017.8265757.

[4] J. Lauenstein, M. Casey, R. Ladbury, H. S. Kim, A. Phan, and A. D. Topper, "Space Radiation Effects on SiC Power Device Reliability," *2021 IEEE International Reliability Physics Symposium (IRPS)*, 2021, doi: 10.1109/IRPS46558.2021.9405180.

[5] K. F. Galloway *et al.*, "Failure Estimates for SiC Power MOSFETs in Space Electronics," *Aerospace*, vol. 5, no. 3, p. 67, Sep. 2018, doi: 10.3390/aerospace5030067.

[6] S. Kuboyama *et al.*, "Thermal Runaway in SiC Schottky Barrier Diodes Caused by Heavy Ions," *IEEE Transactions on Nuclear Science*, vol. 66, no. 7, pp. 1688–1693, Jul. 2019, doi: 10.1109/TNS.2019.2914494.

[7] C. Martinella *et al.*, "Impact of Terrestrial Neutrons on the Reliability of SiC VD-MOSFET Technologies," *IEEE Transactions on Nuclear Science*, vol. 68, no. 5, pp. 634–641, May 2021, doi: 10.1109/TNS.2021.3065122.

[8] D. R. Ball *et al.*, "Estimating Terrestrial Neutron-Induced SEB Cross Sections and FIT Rates for High-Voltage SiC Power MOSFETs," *IEEE Transactions on Nuclear Science*, vol. 66, no. 1, pp. 337–343, Jan. 2019, doi: 10.1109/TNS.2018.2885734.

[9] K. Niskanen *et al.*, "Neutron-Induced Failure Dependence on Reverse Gate Voltage for SiC Power MOSFETs in Atmospheric Environment," *IEEE Transactions on Nuclear Science*, vol. 68, no. 8, pp. 1623–1632, Aug. 2021, doi: 10.1109/TNS.2021.3077733.

[10] D. J. Lichtenwalner *et al.*, "Reliability of SiC Power Devices against Cosmic Ray Neutron Single-Event Burnout," *Materials Science Forum*, 2018. /MSF.924.559 (accessed Apr. 17, 2020).

[11] F. Pintacuda, S. Massett, E. Vitanza, M. Muschitiello, and V. Cantarella, "SEGR and PIGS Failure Analysis of SiC Mosfet," in *2019 European Space Power Conference (ESPC)*, Sep. 2019, pp. 1–5. doi: 10.1109/ESPC.2019.8931999.

[12] L. Xiaowen *et al.*, "Study of heavy ion induced single event gate rupture effect in SiC MOSFETs," *Jpn. J. Appl. Phys.*, vol. 61, no. 8, p. 084002, Jul. 2022, doi: 10.35848/1347-4065/ac7dd4.

[13] N. Für, M. Belanche, C. Martinella, P. Kumar, M. E. Bathen, and U. Grossner, "Investigation of electrically active defects in SiC power diodes caused by heavy ion irradiation," *IEEE Transactions on Nuclear Science*, pp. 1–1, 2023, doi: 10.1109/TNS.2023.3242760.

[14] C. Peng *et al.*, "Experimental and simulation studies of radiation-induced single event burnout in SiC-based power MOSFETs," *IET Power Electronics*, vol. 14, no. 9, pp. 1700–1712, 2021, doi: 10.1049/pel2.12147.

Downloaded from http://dl.asminternational.org/istfa/proceedings-pdf/ISTFA2023/84741/483/662579/istfa2023p0483.pdf
by guest

[15] C. Martinella, S. Race, R. Stark, R. G. Alia, A. Javanainen, and U. Grossner, "High-energy proton and atmospheric-neutron irradiations of SiC power MOSFETs: SEB study and impact on channel and drift resistances," *IEEE Transactions on Nuclear Science*, pp. 1–1, 2023, doi: 10.1109/TNS.2023.3267144.
[16] K. Niskanen *et al.*, "Impact of electrical stress and neutron irradiation on reliability of silicon carbide power MOSFET," *IEEE Transactions on Nuclear Science*, pp. 1–1, 2020, doi: 10.1109/TNS.2020.2983599.
[17] C. Martinella *et al.*, "Impact of Terrestrial Neutrons on the Reliability of SiC VD-MOSFET Technologies," *IEEE Transactions on Nuclear Science*, vol. 68, no. 5, pp. 634–641, May 2021, doi: 10.1109/TNS.2021.3065122.
[18] C. Martinella *et al.*, "Heavy-ion induced single event effects and latent damages in SiC power MOSFETs," *Microelectronics Reliability*, vol. 128, p. 114423, Jan. 2022, doi: 10.1016/j.microrel.2021.114423.
[19] K. Niskanen, H. Kettunen, D. Söderström, M. Rossi, J. Jaatinen, and A. Javanainen, "Proton irradiation-induced reliability degradation of SiC power MOSFET," *IEEE Transactions on Nuclear Science*, pp. 1–1, 2023, doi: 10.1109/TNS.2023.3242829.
[20] R. C. Germanicus *et al.*, "Parametric nano-electrical analysis for SiC junctions of a packaged device," in *2022 IEEE Workshop on Wide Bandgap Power Devices and Applications in Europe (WiPDA Europe)*, Sep. 2022, pp. 1–6. doi: 10.1109/WiPDAEurope55971.2022.9936397.

Downloaded from http://dl.asminternational.org/istfa/proceedings-pdf/ISTFA2023/84741/483/662579/istfa2023p0483.pdf
by guest